International Journal of Applied Earth Observation and Geoinformation 132 (2024) 104043

Contents lists available at ScienceDirect

International Journal of Applied Earth Observation and Geoinformation

journal homepage: www.elsevier.com/locate/jag

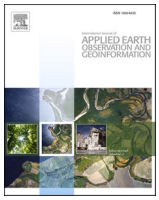

Comparing multispectral and hyperspectral UAV data for detecting peatland vegetation patterns

Yuwen Pang [a,*], Aleksi Räsänen [b,c], Franziska Wolff [d], Teemu Tahvanainen [e], Milja Männikkö [f], Mika Aurela [f], Pasi Korpelainen [d], Timo Kumpula [d], Tarmo Virtanen [a]

[a] Environmental change research unit (ECRU), Ecosystem and Environment Research Program, Faculty of Biological and Environmental Sciences, University of Helsinki, Helsinki, Finland
[b] Natural Resources Institute Finland (Luke), Oulu, Finland
[c] Geography Research Unit, University of Oulu, Oulu, Finland
[d] Department of Geographical and Historical Studies, University of Eastern Finland, Joensuu, Finland
[e] Department of Environmental and Biological Sciences, University of Eastern Finland, Joensuu, Finland
[f] Finnish Meteorological Institute, Helsinki, Finland

ARTICLE INFO

Keywords:
Peatland vegetation mapping
Hyperspectral remote sensing
Geographic object-based image analysis
Random forest

ABSTRACT

Northern peatland vegetation exhibits fine-scale spatial and spectral heterogeneity that can potentially be captured with uncrewed aerial vehicle (UAV) data due to their ultra-high spatial resolution (<10 cm). From this perspective, the contribution of different spectral sensors in mapping various vegetation characteristics has not been thoroughly investigated. We delineated spatial patterns of plant community clusters, plant functional types (PFTs), and selected plant species with UAV hyperspectral (HS), UAV multispectral (MS), and airborne LiDAR (light detection and ranging) topography (TP) data in two northern peatlands. We conducted random forest (RF) regressions in a geographic object-based image analysis (GEOBIA) framework and compared the relative contributions of the different datasets. In the best regression models, the percentage of explained variance was 24–74 % (RMSE:0.24–0.31), 40–90 % (RMSE:0.12–0.41), and 18–90 % (RMSE:0.03–0.40) for plant community clusters, PFTs, and plant species, respectively. The MS-TP combination had, in many cases, the highest performance, while HS-based models had better performance for some plant community clusters, PFTs, and plant species. TP features were useful only in certain situations. Overall, our results suggest that UAV MS imagery combined with TP data outperformed or performed at least almost as well as the models using UAV HS data and while all data combinations are capable for fine-scale detection of vegetation in northern peatlands. A more comprehensive investigations of data processing and methodology selection is needed to conclude if there is an added value of UAV HS data for peatland vegetation monitoring.

1. Introduction

Peatlands are widespread in the northern mid to high latitudes (45–70°N), storing nearly 85 % of the global peatland carbon stock, approximately 550 gigatons (Yu, 2012). These northern peatlands, found in temperate, boreal, and arctic regions, are associated with cool to very cool climates and are particularly vulnerable to climate warming, with Arctic warming being nearly three times the global average (Loisel et al., 2017). Within peatlands, different vegetation communities are found on micro-topographically different surfaces due to moisture and other environmental gradients (Andersen et al., 2011, Baird et al., 2016). Typical microforms and their representative plant communities in northern peatlands are elevated and relatively dry strings with dense vascular plant cover, wet flarks dominated by mosses and sparsely grown graminoids, and intermediate lawns covered by lower and less dense shrubs and forbs (Harris et al., 2020, Rydin and Jeglum, 2013). These microforms create differently patterned string–lawn–flark microtopographies and mosaics and related plant communities (Rydin et al., 2006, Swanson and Grigal, 1988).

A plant community is defined as a group of plant species that live together and have similar environmental requirements. In addition to species identity, plant functional types (PFTs) can be used to characterize the communities (Harris and Baird, 2019, Andersen et al., 2011). PFTs group plants with similar physiological and morphological

* Corresponding author.
E-mail address: yuwen.pang@helsinki.fi (Y. Pang).

https://doi.org/10.1016/j.jag.2024.104043
Received 22 April 2024; Received in revised form 1 July 2024; Accepted 14 July 2024
Available online 18 July 2024

attributes, and categories used in peatlands include deciduous shrubs, evergreen shrubs, forbs, graminoids, *Sphagnum* mosses, wet brown mosses, and feather mosses (Räsänen et al., 2020a, Rupp et al., 2019). Typically, some key plant species can be considered indicators for different microforms (Harris and Baird, 2019), e.g., *Sphagnum fuscum* in hummocks, *Sphagnum fallax* in lawns, and *Sphagnum majus* in flarks (Baird et al., 2016, Rydin and Jeglum, 2013).

To capture spatial patterns of vegetation, uncrewed aerial vehicle (UAV) data with an ultra-high spatial resolution (<10 cm), is needed in the spatially heterogeneous peatlands compared with the coarse spatial resolution remote sensing imagery (Wu et al., 2023, Steenvoorden et al., 2023, Bertacchi et al., 2019). Vegetation communities may still exhibit a high degree of spectral similarity, influencing the optimal remote sensing detection. Several studies have classified peatland vegetation communities using UAV multispectral (MS) data (Diaz-Varela et al., 2018, Simpson et al., 2024, Wolff et al., 2023). Furthermore, the use of hyperspectral (HS) data has been tested in peatlands, and there have been successful applications of handheld (Erudel et al., 2017, Pang et al., 2022) and crewed aircraft (Harris et al., 2015, Szporak-Wasilewska et al., 2021, Middleton et al., 2012, McPartland et al., 2019) HS data. Lately, also studies using UAV HS data have been conducted (Abdelmajeed and Juszczak, 2024), but reports of their use in northern peatlands are still scarce (Zhang et al., 2018, Räsänen et al., 2020b). The few studies have mainly focused on the quantitative derivation of vegetation characteristics, not on delineating the spatial distribution of plant communities or even species. While the potential of HS data has long been suggested, no studies have yet elucidated the relative contribution of UAV HS and UAV MS to characterize peatland vegetation.

Furthermore, using other than optical remote sensing data, such as topography (TP) data derived e.g. from light detection and ranging (LiDAR) has also been found to facilitate the classification of peatland vegetation communities (Beyer et al., 2019, Kaneko et al., 2024), PFTs (Beyer et al., 2019), and even plant species (Li et al., 2017, Hall and Lara, 2022). However, it has not been widely investigated whether the inclusion of TP information impacts differently UAV HS-based than UAV MS-based vegetation pattern detection (Wolff et al., 2023).

We delineated the spatial patterns of plant community types and % cover of PFTs and plant species in two mostly treeless northern boreal peatlands in Finnish Lapland with UAV HS, UAV MS, and TP data. Specifically, we addressed the following research questions: (1) How well can the peatland vegetation characteristics be detected with UAV MS, UAV HS, and TP data? (2) Do HS features improve vegetation detectability (i.e., mappability potential), compared with MS data? (3) Do prediction models benefit from the inclusion of TP information?

2. Materials and methods

We collected two types of UAV data (112-band SPECIM AFX10 HS imagery and 5-band MicaSense RedEdge MS imagery) at two northern peatlands in Finland. We calculated spectral indices to complement the original spectral bands, and we derived eight aerial LiDAR-based TP features. We applied two random forest (RF)-based methods to build regression models and generate vegetation maps (Fig. 1): geographic object-based image analysis (GEOBIA) integrated with (1) default RF and (2) default RF after variable selection using random forest (RF-VSURF).

2.1. Study sites

We studied two open peatland sites, Halssiaapa and Kaamanen, located in northern boreal vegetation zone at 67–69°N in northern Finland (Fig. 2). In both sites, the microclimate and greenhouse gas exchange have been widely studied, e.g., with the eddy covariance

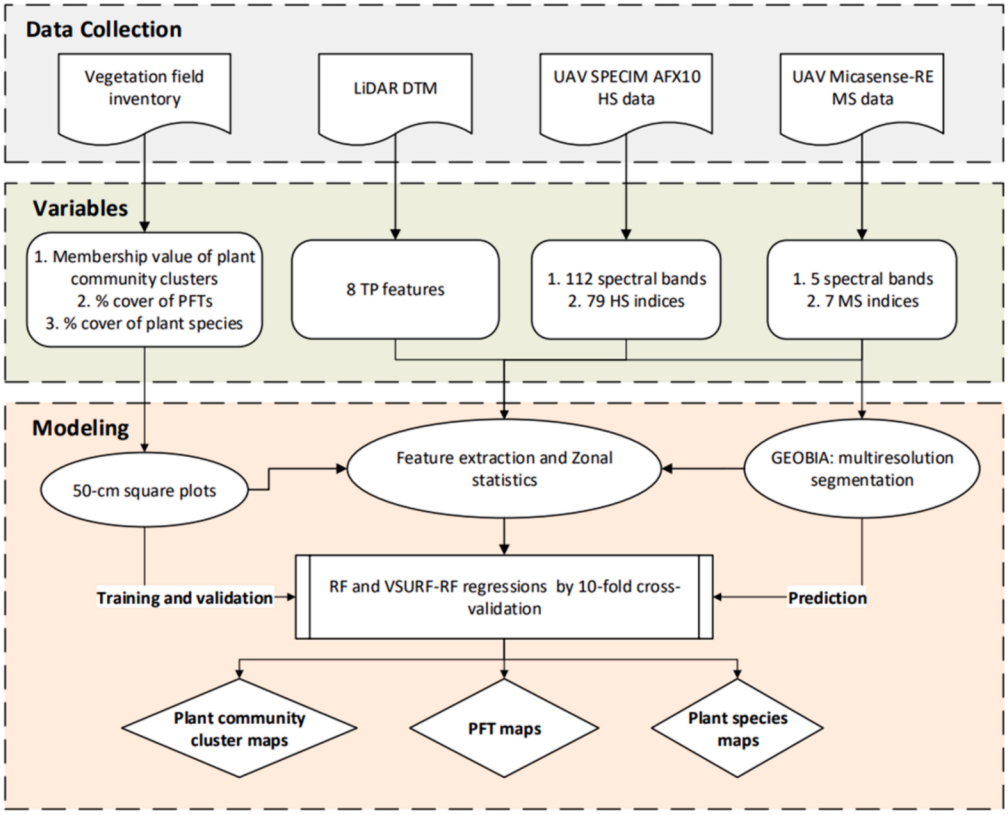

Fig. 1. Workflow of the study. In the figure, LiDAR refers to light detection and ranging, DTM to digital terrain model, UAV to uncrewed aerial vehicle, HS to hyperspectral, MS to multispectral, PFT to plant functional type, TP to topography, GEOBIA to geographic object-based image analysis, and RF to random forest and RF-VSURF to RF after variable selection using random forest.

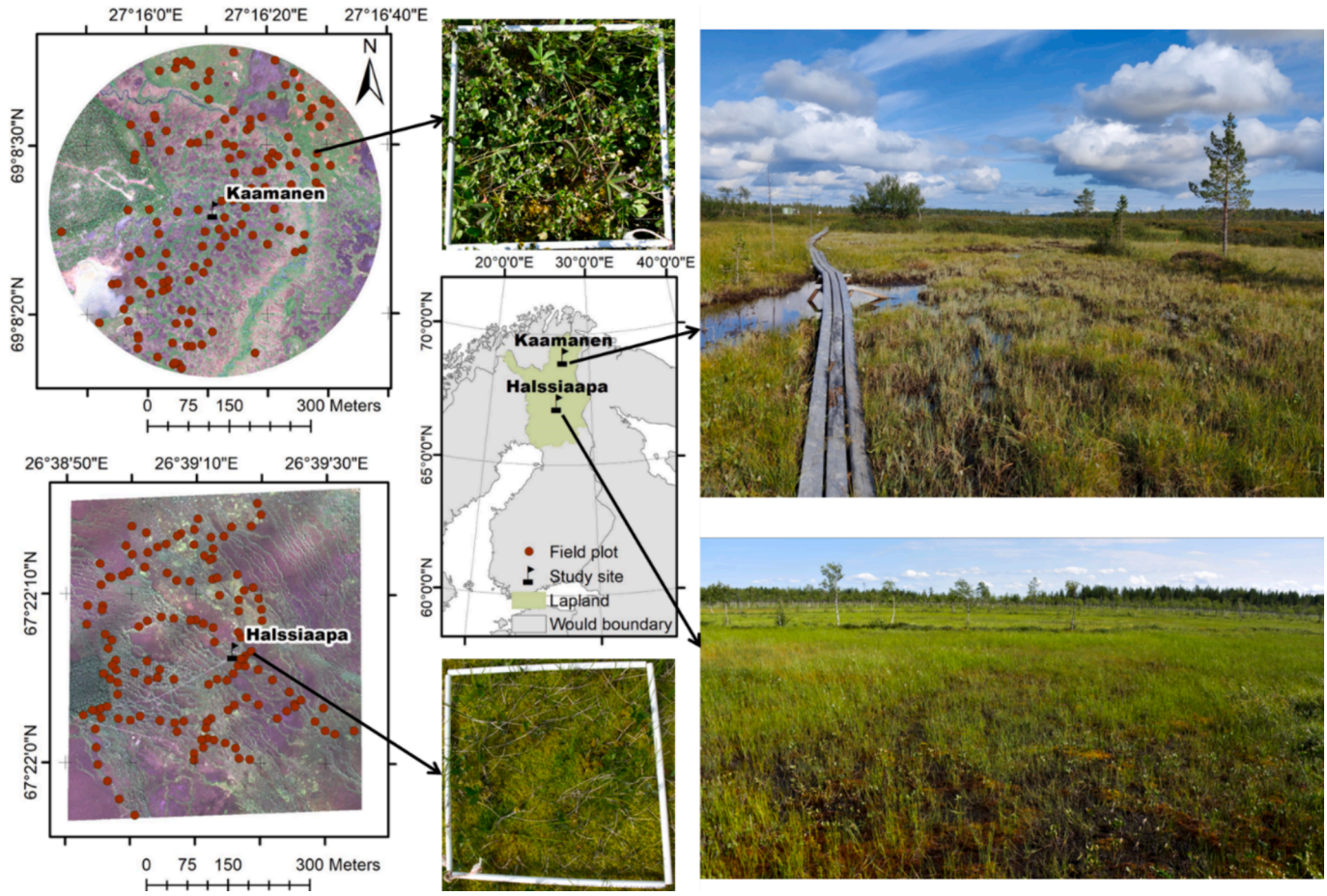

Fig. 2. Locations of study sites and field plots, and photos of the landscape. The base maps of study sites are true colour images (R=668 nm, G=560 nm, B=475 nm) from UAV MicaSense RedEdge-M data, and their collection dates are listed in Table 1.

tower method (Heiskanen et al., 2021, Kou et al., 2022, Linkosalmi et al., 2022). The sites exhibit spatial heterogeneity characterized by variations in microtopography and plant compositions (Räsänen et al., 2020a), providing meaningful sites for ultra-high-resolution UAV-based investigations (Räsänen et al., 2019). Long-term (1991–2020) mean annual temperature and precipitation are 0.2 °C and 539 mm in Halssiaapa and 0.0 °C and 507 mm in Kaamanen, respectively.

The Halssiaapa site (67°22′ N, 26°39′ E, 180 m a.s.l., Fig. 2) is a patterned and open fen with alternating strings, lawns, and flarks, with the mean vegetation height of ca. 0.4 m. Altitudinal differences between strings, lawns and flarks are only tens of centimetres, mostly below half a meter. The narrow (0.5–10.0 m wide), interconnected dry strings are covered by various shrubs, such as *Betula nana*, *Andromeda polifolia,* and *Vaccinium oxycoccos*, and a few stunted trees, mostly *Betula pubescens* and *Pinus sylvestris*. Wet flarks are dominated by wet brown mosses (e.g., *Sarmentypnum procerum*) and sedges (e.g., *Carex limosa*), and intermediate lawns are characterized by *Sphagnum* mosses (e.g., *S. warnstorfii*) and forbs (e.g., *Menyanthes trifoliata*). Halssiaapa is flooded during spring (May–early June), with the water table being a few centimetres above the ground surface in flarks. Some periodical flooding might occur also later in the season after heavy rains (Mörsky et al., 2012).

The Kaamanen site (69°8′ N, 27°16′ E, 155 m a.s.l., Fig. 2) has a mean vegetation height of ca. 0.3 m and is characterized by a strong mosaic pattern of hummock strings and wet flarks. The strings are up to 1 m high and 10 m long and their vegetation consist of evergreen shrubs, like *Empetrum nigrum*, *Rhododendron tomentosum,* and *Vaccinium vitis-idaea*, and forbs, such as *Rubus chamaemorus.* Wet flarks are flooded in the spring and have some open water cover during most of the seasons. They are primarily occupied by partly submerged wet brown mosses, specifically *Scorpidium scorpioides*, along with sparsely growing *Carex* (e.g., *C. limosa* and *C. chordorrhiza*) and *Trichophorum* species (e.g., *T. alpinum* and *T. cespitosum*). At the string margins, shrubs dominate, and *Sphagnum* carpets are also found (e.g., *S. lindbergii*). Pine forests (*Pinus sylvestris*) occur around the fen borders. In the transition zone, there are pine bogs characterized by various shrubs and forbs, while their ground layer is covered by feather mosses (e.g., *Pleurozium schreberi*) and *Sphagnum* mosses (e.g., *S. fuscum*). There is also a stream running through the area with its margins covered by tall sedges and deciduous shrubs (e.g., *Salix* spp., *Vaccinium uliginosum*). In addition to precipitation, Kaamanen receives water through surface flow from the surrounding areas, particularly during the spring high-flow period. Owing to their elevated surfaces, the strings exhibit ombrotrophic characteristics, primarily relying on precipitation for water and nutrients. Thin ice lenses endure within the well-insulated hummocks until late summer (Maanavilja et al., 2011).

2.2. Vegetation field inventories and community analyses

We conducted vegetation inventories between the last week of July and the first week of August, corresponding to the peak vegetation growing season (Table 1). According to our existing land cover maps (Räsänen et al., 2020b, Räsänen and Virtanen, 2019), we sampled 135 and 132 square plots of 0.25 m^2 in Halssiaapa in 2022 and in Kaamanen in 2021, respectively, using the stratified random sampling method.

During the inventories, we identified vascular plants at the species level and mosses at the genus or species level and estimated their %-cover. We used non-metric multidimensional scaling (NMDS) and fuzzy k-medoid (FKM) clustering to translate the plant inventory data

Table 1
Summary of remote sensing data.

Site	Date of acquisition	UAV data	Spatial resolution [m]	Covered area [ha]	No. of layers
Kaamanen	29 Jul 2021	Specim AFX10	0.1	29.21	191: 112 spectral bands and 79 HS spectral indices (Tables S3&S5 in Appendix 1)
		MicaSense RedEdge-M	0.08		12: 5 spectral bands and 7 MS spectral indices (Tables S4&S6 in Appendix 1)
	Aug 1 2018	LiDAR DTM	2		8: elevation, slope, TWI and 5 TPIs (5, 10, 20, 50, and 100 m distance)
Halssiaapa	24 Jul 2022	Specim AFX10	0.09	31.46	Same as the Kaamanen site
		MicaSense RedEdge-M	0.08		Same as the Kaamanen site
	Aug 20 2018	LiDAR DTM	2		Same as the Kaamanen site

Abbreviations: HS=hyperspectral; MS=multispectral; DTM=digital terrain model; TWI=topographical wetness index; TPI=topographical position index.

into plant community clusters (see Figure S1 in Appendix 1). To do this, we first conducted Wisconsin double standardization and square root transformation and calculated Bray–Curtis (BC) distances on inventory data. Second, we performed NMDS to BC matrix by running 20 random starts to ensure a scaling stress value below 0.1 and restricted the iteration to four dimensions in R using the package vegan (Oksanen et al., 2020). Third, we searched for the optimal cluster number between 1 and 10 by maximizing the silhouette width (Campello and Hruschka, 2006) and then applied the determined number to FKM clustering with a membership exponent of 1.5 using the R package fclust (Ferraro et al., 2019). We obtained three and four clusters in Halssiaapa and Kaamanen, respectively. We also ran an indicator species analysis for the cluster results, using the indicator value method with 999 random permutations and the R package indicspecies (De Caceres et al., 2020). After interpretation, we named the clusters by their ground surface microforms: string, flark, and lawn in Halssiaapa, and string top, wet flark, string margin, and *Sphagnum* lawn in Kaamanen (plant species compositions, including indicator species, are given in Tables S1&S2 in Appendix 1).

In addition, we grouped the plant species into seven PFTs: deciduous shrubs, evergreen shrubs, forbs, graminoids, wet brown mosses, feather mosses, and *Sphagnum*, as well as selected 15 and 17 dominant or common plant species in Halssiaapa and Kaamanen, respectively (Tables S1&S2 in Appendix 1).

2.3. Remote sensing data and image processing

We collected UAV HS and MS data simultaneously with field inventories (Table 1). The HS imagery was acquired with a SPECIM AFX10 sensor mounted on a DJI Wind 4 UAV with a flight altitude of 117 m and a field of view (FOV) of 38°. During the flights, we configured the sensor with a 4 (spectral option) × 1 (spatial option) binning mode, resulting in 112 spectral bands from a wavelength range of 400–1000 nm (Table S3 in Appendix 1). We geometrically calibrated the imagery using the ENVI plug-in CaliGeoPro (Specim Limited, Oulu, Finland); we performed the radiometric calibration by the empirical line method (Wang and Myint, 2015) using three photographed MosaicMill reflectance panels (Altisense Ltd.) with 0.5 m side length in 0 %, 2 %, and 9 % reflectance. In Kaamanen, we did not have reflectance panels, so we used radiance instead of reflectance data.

The 5-band MS imagery was acquired by the MicaSense RedEdge-M sensor mounted on a DJI Phantom 4 UAV with a flight altitude of 70 m and a focal length of 5.5 mm at 47.2° FOV, resulting in 1280 × 960-pixel photos (Table S4 in Appendix 1). The sensor is also paired with a downwelling light sensor that records the incident/ambient light measurements above and is used to produce reflectance images. We implemented the geometric and radiometric calibration via Pix4D Pro. The HS and MS images were captured temporally close to each other, under predominantly windless and clear weather conditions around noon. However, a few clouds were occasionally present during the flights.

Spectral indices, derived from spectral reflectance properties, linking to various plant biophysical properties (e.g., leaf area, leaf pigments, and vegetation cover and moisture) and health of vegetation, are commonly used to predict vegetation characteristics and distinguish vegetation types (Dronova et al., 2021). We calculated 79 and 7 spectral indices for MS and HS data, respectively (Table 1 and Tables S5&S6 in Appendix 1), in R using packages of raster (Hijmans, 2018) and hsdar (Lehnert et al., 2019).

Besides the optical UAV data, we utilized the LiDAR-based digital terrain model (DTM) with a 2 m resolution from the National Land Survey of Finland (NLSF) via open data service. The original LiDAR data contains 3D point clouds with a point density of 0.5 points per square metre. We derived eight TP features from the DTM, including elevation in metres, slope in degrees, topographical wetness index, and TP position index with five different neighbourhood radii in the SAGA GIS 7.8.2 (Conrad et al., 2015) (Table 1).

2.4. Geographic object-based image analysis and modelling

We performed the regressions with a GEOBIA approach, which has been demonstrated to effectively avoid the salt-and-pepper effect common in pixel-based classifications (Berhane et al., 2018, Du et al., 2021). In GEOBIA, images are analysed at the object or segment level, grouping neighbouring pixels with similar spectral, spatial, and contextual characteristics to reduce noise and variability within individual pixels (Hossain and Chen, 2019). GEOBIA usually consists of two main steps: (1) image segmentation and (2) feature extraction and image analysis (Hossain and Chen, 2019, Blaschke et al., 2014). Segmentation is the basis of GEOBIA; it divides the image pixels into spatially contiguous and homogeneous objects and significantly affects the subsequent image analysis (Kotaridis and Lazaridou, 2021), i.e., the RF regression modelling in this study.

We used the 5-band UAV MS data in the multi-resolution segmentation (MRS) (Baatz and Schäpe, 2000), in TerraView 5.6.4. MRS has four main parameters: the minimum segmentation size, the spectral similarity threshold, and the weight of colour and compactness; the first two metrics control the size of segments, and the other two impacts the shape of segments (Witharana and Civco, 2014, Räsänen et al., 2013). After several trials and based on visual interpretation, we set the parameters to 150 (0.96 m^2 area), 0.15, 0.8, and 0.5, respectively (segmentation results are shown in Figure S2 in Appendix 1).

We extracted the remote sensing features (Table 1) and applied them to the segments and the vegetation plots. We used the plot data for training and validation and the segment data for constructing the vegetation maps. To compare the contribution of specific RS features, we used four input options: (1) 191 HS layers (HS), (2) 191 HS layers and 8 TP layers (HS+TP), (3) 12 MS layers (MS), and (4) 12 MS layers and 8 TP layers (MS+TP) (Table 1).

After feature extraction, we performed default RF regressions (Breiman, 2001) without or with variable selection RF-VSURF (Genuer et al., 2015). RF employs ensemble learning and majority voting, mitigates overfitting and balances outliers or erroneous predictions from individual trees, resulting in more stable and reliable predictions. It has

successfully been used in remote sensing mapping applications (Jafarzadeh et al., 2022, Prentice et al., 2021, Maxwell et al., 2018). By selecting a subset of relevant variables from a larger set, VSURF enhances model interpretability, reduces dimensionality that is present particularly in HS datasets, and often improves model fit (Putkiranta et al., 2024, Wengert et al., 2022).

Previous studies have suggested that a large number of trees and a small number of split variables yield optimal RF models (Ma et al., 2015, Belgiu and Dragut, 2016). Therefore, for each RF regression run, we set the number of trees to 500 and the number of splits to 1/3 of the number of input RS predictors, following the default setting given by Liaw and Wiener (2002) within the R package randomForest. We proceeded RF-VSURF as follows. First, we conducted VSURF via the R package through a three-step procedure: (1) ranking all variables according to their importance in RF runs, (2) nesting RF models involving the most important variables from the first step, and selecting the model with the lowest OOB (out-of-bag) error, and (3) stepwise selection of the remaining variables, whereby additional variables were only included when the OOB error decreased significantly compared to the average variation obtained by adding noisy variables (Genuer et al., 2015). Second, we run RF with VSURF selected variables. Overall, we compared regression model performance between RF without variable selection and RF with VSURF to determine whether variable reduction enhances the model fit.

For validation, we implemented a 10-fold cross-validation to compute three validation parameters: the percentage of explained variance (pseudo-R^2, 1 − (mean squared error)/variance(response)), MAE (mean absolute error), and RMSE (root mean square error). We calculated the feature importance rate using Gini importance, also known as mean decrease impurity, a commonly used method for measuring feature importance in machine learning (ML) models (Behnamian et al., 2017). Gini importance quantifies each feature's contribution to the model by assessing how much it decreases impurity in a decision tree split. This method provides a clear and interpretable metric for feature importance, allowing us to identify which features play the most significant roles in our regression models. Due to the rather high computational demands, we built a Python environment, including the main modules of rasterio and scikit-learn (Pedregosa et al., 2011), to perform feature extraction and RF analysis on CSC's Puhti supercomputer (https://www.csc.fi/).

3. Results

3.1. Assessing models by different RS options

3.1.1. Model performance

RF and RF-VSURF had relatively similar regression performance, with the performance varying among the four types of RS datasets, the two peatland sites, and the three vegetation categories (Fig. 3, Table 2). In Halssiaapa, the percentage of variance explained was 40–55 % via RF and 42–62 % via VSURF, whereas in Kaamanen, it was 24–44 % via RF and 25–47 % via VSURF (Fig. 3). With the two RF-based regression approaches, Halssiaapa showed better predictions for plant community clusters (50–54 %) and PFTs (51–57 %) compared to plant species (44–48 %). In Kaamanen, plant community clusters (36–42 %) were better predicted than PFTs (28–34 %) and plant species (28–33 %).

The variance explained rate of vegetation categories varied widely among the four RS models, indicating that no single RS option was optimal in all cases, and generally there was not much difference between model types. Nevertheless, MS+TP had on average the highest variance explained among vegetation categories. Specifically, HS+TP models were the best for predicting plant community clusters and plant species in Halssiaapa; MS+TP models for PFTs in Halssiaapa and plant species in Kaamanen; MS models for plant community clusters in Kaamanen; and HS models for PFTs in Kaamanen. Additionally, the modelling performance for different datasets was similar for RF and RF-VSURF models, with HS models performing slightly better with RF-VSURF than with RF. For simplicity, and to reduce the amount of produced maps, only RF-based models were in the end adopted for producing the vegetation maps (Fig. 3, Table 2).

According to RF regressions, the variance explained rates varied widely among vegetation characteristics, with MS models generally better than HS models on average (Fig. 4). However, HS models achieved higher explained variance rates than MS models in some cases. Some characteristics had high model performance (explained variance > 70 %) such as string fens, forbs, and *Sphagnum* in Halssiaapa, and evergreen shrubs and *Menyanthes trifoliata* in Kaamanen. HS models improved the detection of lawns and *Rhododendron tomentosum* in

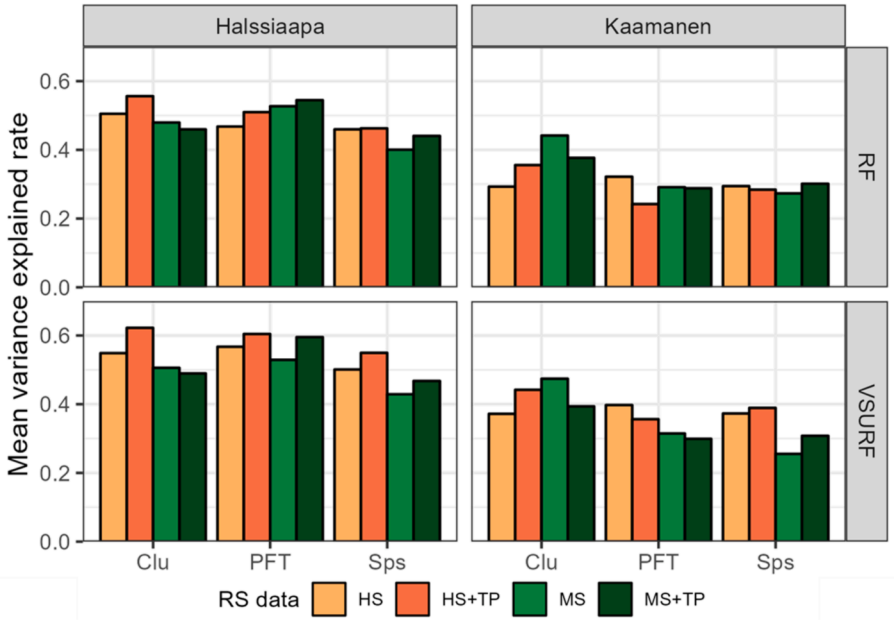

Fig. 3. Model performance comparison between random forest (RF) and variable selection using random forest (VSURF) across three vegetation categories: plant community cluster (Clu), plant functional type (PFT), and target plant species (Sps). Models were built using four types of RS data: (1) HS=191 hyperspectral (HS) layers; (2) HS+TP=191 HS and 8 topography (TP) layers; (3) MS=12 multispectral (MS) layers; and (4) MS+TP=12 MS and 8 TP layers.

Table 2
Mean RMSE and MAE of regression models using random forest (RF) and variable selection using random forest (VSURF) for plant community cluster (Clu), plant functional type (PFT), and target plant species (Sps), across four RS data options: (1) HS=191 HS layers; (2) HS+TP=191 HS layers and 8 TP layers; (3) MS=12 MS layers; and (4) MS+TP=12 MS layers and 8 TP layers.

Regression	RS data	RF		VSURF		RF		VSURF	
		RMSE Halssiaapa	MAE	RMSE	MAE	RMSE Kaamanen	MAE	RMSE	MAE
Clu	HS	0.267	0.210	0.267	0.211	0.329	0.275	0.320	0.267
	HS+TP	0.263	0.214	0.260	0.209	0.306	0.252	0.292	0.238
	MS	0.262	0.221	0.262	0.220	0.318	0.272	0.316	0.272
	MS+TP	0.263	0.221	0.264	0.222	0.293	0.245	0.292	0.243
PFT	HS	0.245	0.181	0.234	0.171	0.359	0.271	0.352	0.262
	HS+TP	0.231	0.171	0.219	0.159	0.353	0.270	0.339	0.258
	MS	0.233	0.170	0.233	0.169	0.379	0.292	0.375	0.288
	MS+TP	0.226	0.162	0.219	0.153	0.345	0.266	0.345	0.264
Sps	HS	0.148	0.094	0.143	0.089	0.178	0.116	0.175	0.111
	HS+TP	0.145	0.093	0.140	0.087	0.175	0.114	0.170	0.108
	MS	0.137	0.084	0.135	0.082	0.176	0.113	0.178	0.112
	MS+TP	0.138	0.087	0.136	0.082	0.171	0.112	0.171	0.109

Halssiaapa as well as evergreen shrubs, forbs, graminoids, and *Trichophorum* spp. in Kaamanen. TP features also increased model performance in some cases, particularly for lawns, feather mosses, *Carex paupercula,* and *Comarum palustre* in Halssiaapa and for *Sphagnum* lawns, *Carex limosa,* and *Menyanthes trifoliata* in Kaamanen. However, in other cases, models with TP features were worse than the corresponding spectral-only models.

3.1.2. Feature importance

HS indices had on average the highest importance in HS+TP options, followed by certain HS bands, while in MS+TP options, TP features were the most important in Kaamanen and MS features in Halssiaapa (Fig. 5).

3.2. Vegetation maps

We used the HS+TP and MS+TP datasets to generate the final vegetation maps (examples in Fig. 6&Fig. 7, all maps in Appendices 2–3). While both models captured the spatial patterns of vegetation, HS+TP-based maps typically delineated more details than MS+TP maps. For example, the HS+TP model clearly distinguished the lawn in the northeast corner of Halssiaapa and depicted *Menyanthes trifoliata* in the centre of Kaamanen. Based on the maps, vegetation had different spatial patterns at study sites, as Halssiaapa consisted of merged linear strings alternating with lower and wetter flarks and patches of lawn, while Kaamanen had maze-like strings surrounded by a matrix of flarks. Moreover, different PFTs and plant species concentrated on specific microforms such as feather mosses (including *Dicranum* spp., *Hylocomium splendens*, *Plagiomnium* spp., *Pleurozium schreberi,* and *Polytrichum strictum*) growing along strings in Halssiaapa and the dense evergreen shrubs in string tops in Kaamanen.

4. Discussion

4.1. Model performance and differences between sites and characteristics

In the regression models, the percentage of variance explained varied markedly between sites and vegetation categories, where plant community clusters, PFTs, and plant species were on average explained by 24–74 %, 40–90 %, and 18–90 %, respectively, with RF regression models. In most cases, the MS+TP setting performed well, although in some cases the HS settings can also achieved good performance (Fig. 3 & Fig. 4).

Differences in model performance between sites may be due to distinct landscape patterns, i.e., linear strings in Halssiaapa vs. string mazes in Kaamanen, influencing the modelling processes. Another explanation for the relatively poor modelling performance in Kaamanen may be the use of radiance instead of reflectance data for UAV HS. The magnitude of spectral radiance reflects the amount of incident solar radiation (spectral irradiance) reaching the target and is impacted by various factors such as the solar zenith angle, atmospheric conditions, water vapour and aerosol loading levels (Peddle et al., 2001). Reflectance or atmospherically calibrated spectral data are commonly implemented in UAVs and other remote sensing applications (Salamí et al., 2014, Assmann et al., 2019). Nevertheless, radiometric data can still be used as a reliable input for land cover classification, but the preprocessing of radiometric data and the approach of image analysis can greatly affect the accuracy and reliability of the output results (Plaza et al., 2009, Aasen et al., 2018).

We also found that plant community clusters and PFTs were predicted better than plant species (Fig. 4), although some *Carex* species (e.g., *C. limosa* and *C. chordorrhiza*) had explained variance of over 50 % (Fig. 4). Consistent with previous findings (Pang et al., 2022, Räsänen et al., 2020a), some plant community clusters and PFTs were relatively well predicted, e.g., strings and *Sphagnum* in Halssiaapa and string tops and margins and evergreen shrubs in Kaamanen (Fig. 4), which is attributed to the higher spectral and topographic separability of these characteristics.

Peatland vegetation patterned along the environmental gradient, e.g., the hydrology and microtopography, the detectability of PFTs and plant species was also related to plant community clusters, leading to shrubs (e.g., *Rhododendron tomentosum*) and forbs (e.g., *Rubus chamaemorus*) in strings having good predictions in Halssiaapa, and feather mosses in string tops being relatively well modelled in Kaamanen. Moreover, influenced by vegetation cover proportion and plant composition (Tables S1&S2 in Appendix 1), the explained variance of PFTs and plant species varied greatly between sites, with wet brown mosses and *Sphagnum* well captured only in Halssiaapa and feather mosses in Kaamanen. In addition, for some less abundant species or plant communities, especially if they are also rare, field data may be insufficient and unrepresentative.

4.2. Comparison of hyperspectral vs. Multispectral

Although some previous results have highlighted the benefits of using HS data, e.g., for predicting fractional covers of PFTs (Zhang et al., 2018) and producing habitat distribution maps of peatlands (Szporak-Wasilewska et al., 2021), we did not see HS generally improving model performance relative to MS. In some cases, HS models performed even worse (Fig. 3 & Fig. 4). However, supporting a recent finding by Arasumani et al. (2023), who reported that spaceborne HS data promoted fractional cover predictions of two graminoid species, *Phragmites australis* (Common Reed) and *Typha* spp. (Cattail), our results indicated that HS improved the model performance for some *Carex* species (Fig. 4).

Another issue long discussed is that plant communities have fairly

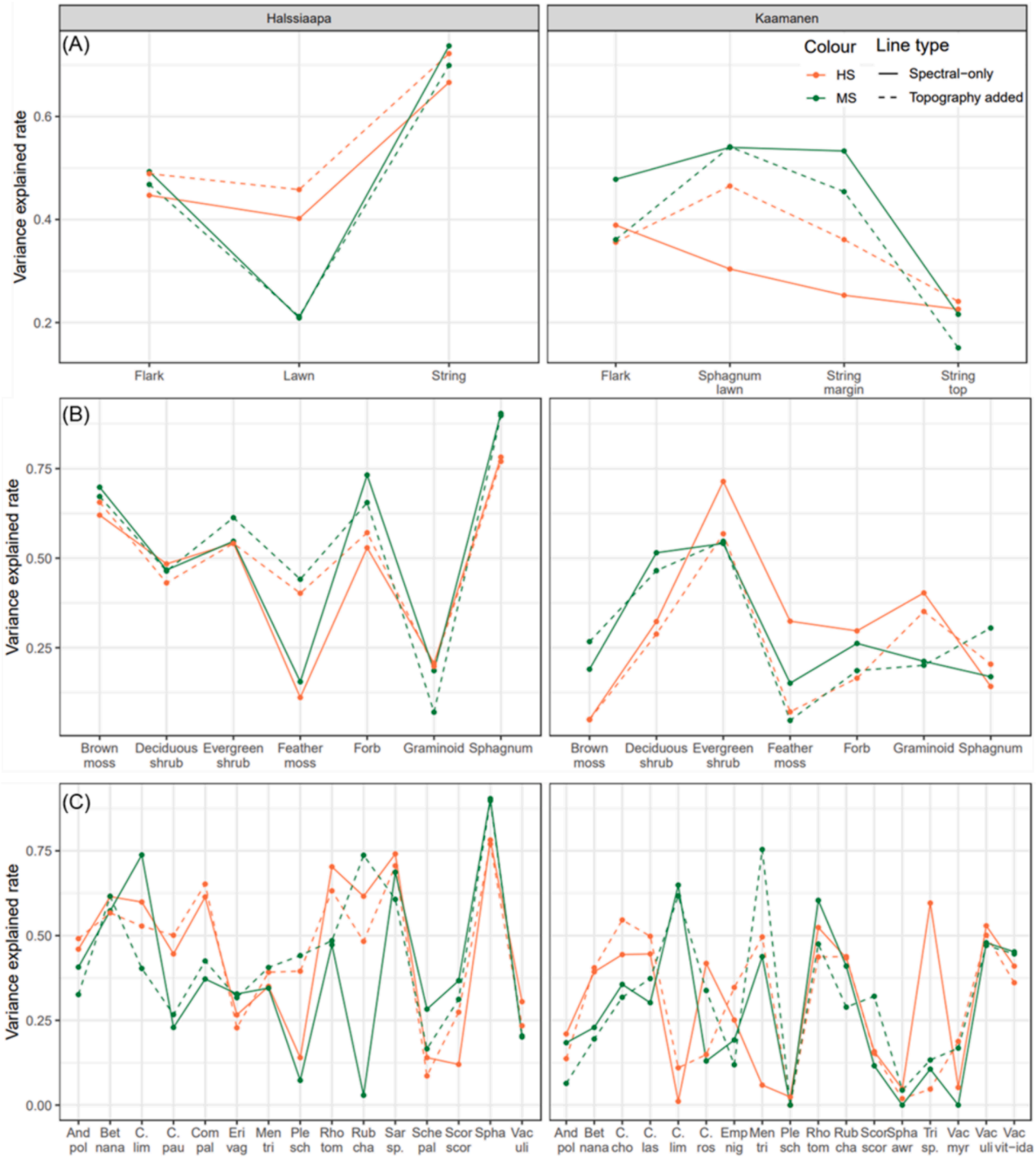

Fig. 4. RF Model performance of vegetation characteristic at two sites: (A) plant community clusters, (B) plant functional types, and (C) plant species, by four RS data options: HS or MS, spectral-only or added TP layers. The full names of plant species are given in Tables S1&S2, and the RMSE and MAE of models are given in Tables S7&S8 in Appendix 1.

similar spectral responses in peatland environments, causing great spectral confusion and hampering spectral discrimination (Zhou et al., 2021, Adam et al., 2010). The high data dimensionality and associated noise of HS data possibly hinder rather than facilitate plant species separation. For example, Kupkova et al. (2023) noted no significant differences between UAV MS and HS for discriminating tundra grass species. Nevertheless, we identified some prominent HS bands and indices that have high importance in the models (Fig. 5), supporting the conclusions of a literature review on HS plant classification (Hennessy et al., 2020). Furthermore, in HS+TP models, the most important variables were generally HS variables whereas in MS+TP models, TP variables were among the most important. Overall, our results suggest that there is no extensive added value in incorporating UAV HS data in optimal peatland vegetation practices, but some HS spectral indices (Fig. 5), e.g., Carter 3 (R605/R760, (Carter, 1994)) and CRI 1 (Carotenoid Reflectance Index 1, 1/R515 − 1/R550, (Gitelson et al., 2002)), were generally beneficial at both sites. However, the complex structure of HS compared to MS information might require a more extensive experimenting of data processing that can also be beneficial for the MS data, for example advanced atmospheric corrections (Marcello et al.,

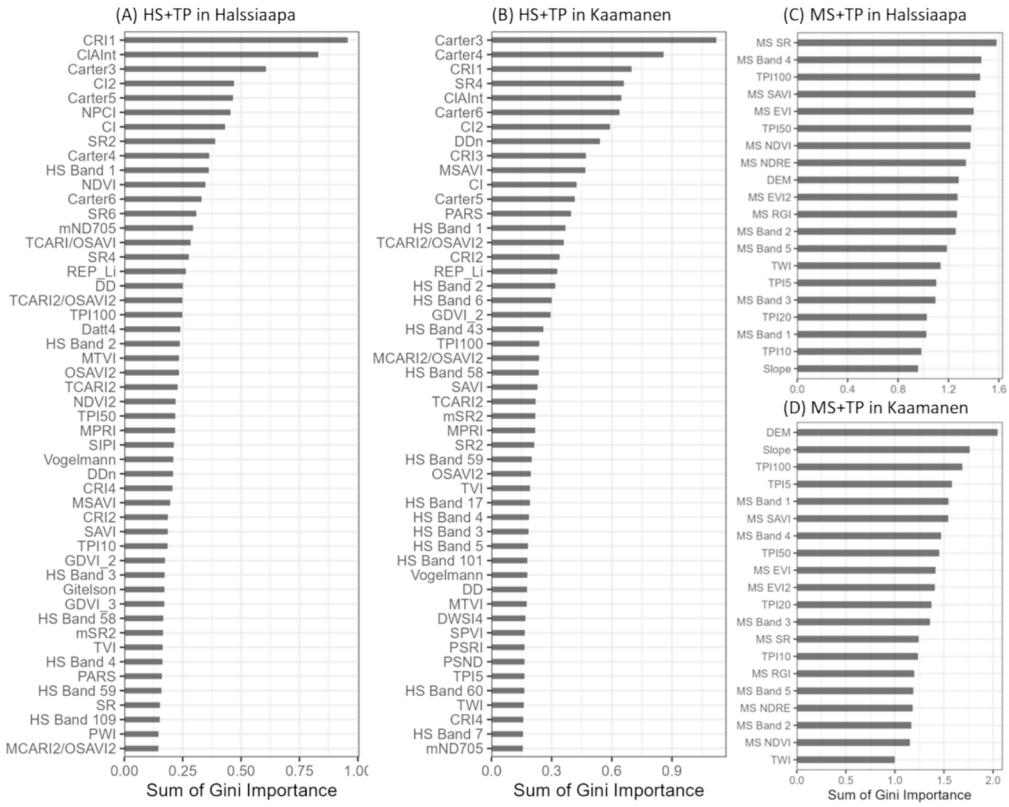

Fig. 5. Sum of Gini importance scores of all regressions by HS+TP (a,b) or MS+TP (c,d) RS data settings at two sites. The figure illustrates the top 50 most important features of HS+TP and all features of MS+TP settings. For the full list and detailed information on all RS features, see Table 1 and Tables S3–S6 in Appendix 1.

2016) and additional steps including different spectral reduction and unmixing techniques (Li et al., 2022, Borsoi et al., 2021). While our data processing has been adequate, it regardless might have not leveraged the full potential of narrow-band hyperspectral information for vegetation modelling. In this context, using MS data offers the clear advantage of easier data collection and processing.

4.3. Role of topography data

Several studies have demonstrated that integrating optical imagery and LiDAR data can improve vegetation mappings in multiple ecosystems such as wetland vegetation communities (Wang et al., 2023), PFTs, and plant species in grasslands (Hall and Lara, 2022) and peatland habitat types (Szporak-Wasilewska et al., 2021). According to our results, however, we argue that the relative contribution of TP features is limited and only significant for some cases (Fig. 3-Fig. 5). TP features allow distinguishing plant community clusters with similar spectral behaviour but different microtopographic positions. Likewise, for PFTs and plant species detection, we further suggest the advantages of TP in terms of presenting micrographic information. For instance, including TP was particularly beneficial for feather mosses (e.g., *Pleurozium schreberi*), which occur along strings and under pines, and forbs *Comarum palustre* and *Menyanthes trifoliata*, which have a high presence in especially lawns. These findings are in contrast to previous studies (Kopecky et al., 2021, Hall and Lara, 2022, Marcinkowska-Ochtyra et al., 2018, Durgan et al., 2020), which have mainly emphasized LiDAR-derived TP features complementing spectral data. We also found that the relative benefit of TP data was approximately similar for HS and MS-based models. The spatial resolution difference between UAV (0.08–0.1 m) and DTM (2 m) data might explain the limited aid offered by adding TP features. However, the incorporation of TP data seems to have at least some value, and if TP had higher spatial resolution, it might have helped even more.

4.4. Limitations and next steps

The produced vegetation maps allow us to see the patterns and presence of vegetation types within peatlands and further understand the changes such as fen–bog transition (Kolari et al., 2021, Wolff et al., 2023) and disturbances (Li et al., 2024, Lovitt et al., 2018). The detailed information on peatland vegetation spatial patterns strengthens the detection and modelling of biological and biogeochemical parameters that use vegetation properties as input data, e.g., leaf area index, biomass, and greenhouse gases (Assiri et al., 2023, McPartland et al., 2019, Hoyos-Santillan et al., 2019).

We calculated spectral properties from the UAV HS and MS data, i.e., bands and indices and TP features for building regressions and generating vegetation maps, without exploring other spatial characteristics. However, some studies have shown that a sub-metre spatial resolution is most effective for achieving good peatland vegetation mapping (Räsänen and Virtanen, 2019, Steenvoorden et al., 2023). In addition, phenological information offers another perspective that facilitates accurate vegetation detection as multi-temporal data has been shown the increase model performance (Pang et al., 2022, Wu et al., 2023). We conducted only one-time UAV flights, but UAV data collection can be repeated regularly over time; therefore, future research could include UAV data about vegetation dynamics and include it in prediction models (Wu et al., 2023). However, when conducting UAV missions, it is critical to weigh the trade-offs between spatial coverage and image acquisition cost relative to the research objectives.

Future research could also evaluate the effectiveness of combining UAV HS and MS data with coarser scale products to develop approaches to upscale vegetation information across larger spatial extents (Villoslada et al., 2024). Further examination could also be put on fusing UAV-based optical data with vegetation height models derived from structure-from-motion or LiDAR. Integrating different types of remote sensing data, including UAV and synthetic aperture radar (SAR), could

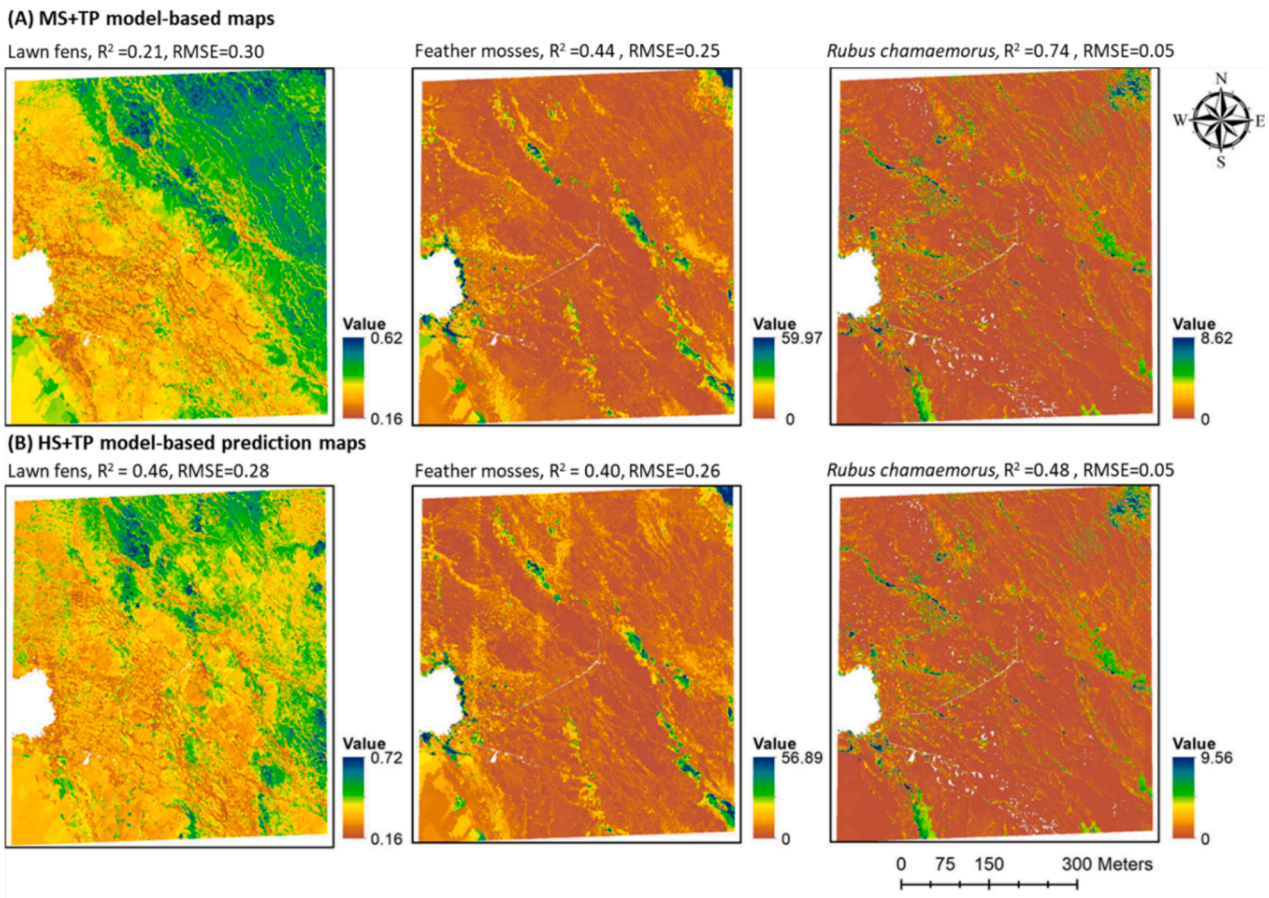

Fig. 6. Example vegetation maps based on (A row) MS+TP and (B row) HS+TP models in Halssiaapa. Other predicted maps are shown in Appendix 2.

also provide comprehensive insights into peatland research (Szporak-Wasilewska et al., 2021, Wang et al., 2023, Isoaho et al., 2024, Räsänen et al., 2022). On the other hand, fieldwork for collecting field reference data is time-consuming and sometimes challenging in peatlands, necessitating well-designed, representative, and balanced sampling. Therefore, establishing a comprehensive framework to process and analyse multi-scale cross-platform data is essential for effectively deriving peatland vegetation characteristics and optimizing the need for fieldwork (Oldeland et al., 2021).

Moreover, we compared UAV HS and UAV MS data only with one ML algorithm (i.e., RF with and without variable selection). Contrary to our expectations, the differences between models with and without variable selection were generally quite small. Even though the selected variable selection method (VSURF) reduces the dimensionality and redundancy in the data, the models with VSURF did not perform largely better than models without it even with highly multidimensional HS data. On the other hand, deep learning (DL) algorithms could facilitate image and statistical analysis to reveal the strengths of HS data since DL can effectively handle high-dimensional data (Dahiya et al., 2023). We briefly experimented with one DL method, namely a feedforward neural network, and preliminary tests did not show a significant improvement in HS or MS models and did not change our conclusions about the relative performance of different datasets (Table S9 in Appendix 1). In addition, the drone data processing steps (including training data generation) led to the best results for the ML model, while the DL model involved different image processing steps, especially for the HS dataset, which further complicated the comparison (Zhang and Zhang, 2022). Therefore, more comprehensive studies are needed in the future to draw more reliable conclusions about whether HS outperforms MS in different landscapes, which should consider not only the choice of methods, such as ML and DL with more complex architectures, but also the incorporation of other data processing techniques.

5. Conclusions

We explored the use of multi-source UAV data in detecting various peatland vegetation characteristics via an RF-integrated GEOBIA approach in two northern peatlands. For the first time, we compared the relative contribution between UAV HS and MS data for predicting three peatland vegetation categories: plant communities, PFTs, and plant species; according to the average performance of the best model, the variance explained was 44–56 %, 32–55 %, and 30–45 %, respectively, with RF regression models at the two sites. Based on our findings, we cannot suggest a single optimal data combination for vegetation pattern detection, as large differences existed between sites and vegetation characteristics about which predictor data functioned the best. In many situations, MS models functioned better than HS models, but for some vegetation characteristics, HS improved the model performance relative to MS. Additionally, integrating TP features improved model performance only in some cases, particularly benefiting MS+TP models. Although in our case, UAV HS was not as advantageous as we expected, this does not mean that HS has no benefits for vegetation monitoring in another case. Instead, we emphasize that the adoption of UAV HS, UAV MS, and TP data depend on the specific site conditions and landscapes. Our study suggests that the fusion of UAV MS and TP data may be an effective combination in most peatland vegetation situations. However, more comprehensive studies on the use of UAV HS, including consideration of data processing and methodological choices, are needed to understand the benefits of added spectral information for spectrally complex and spatially heterogeneous peatland ecosystems.

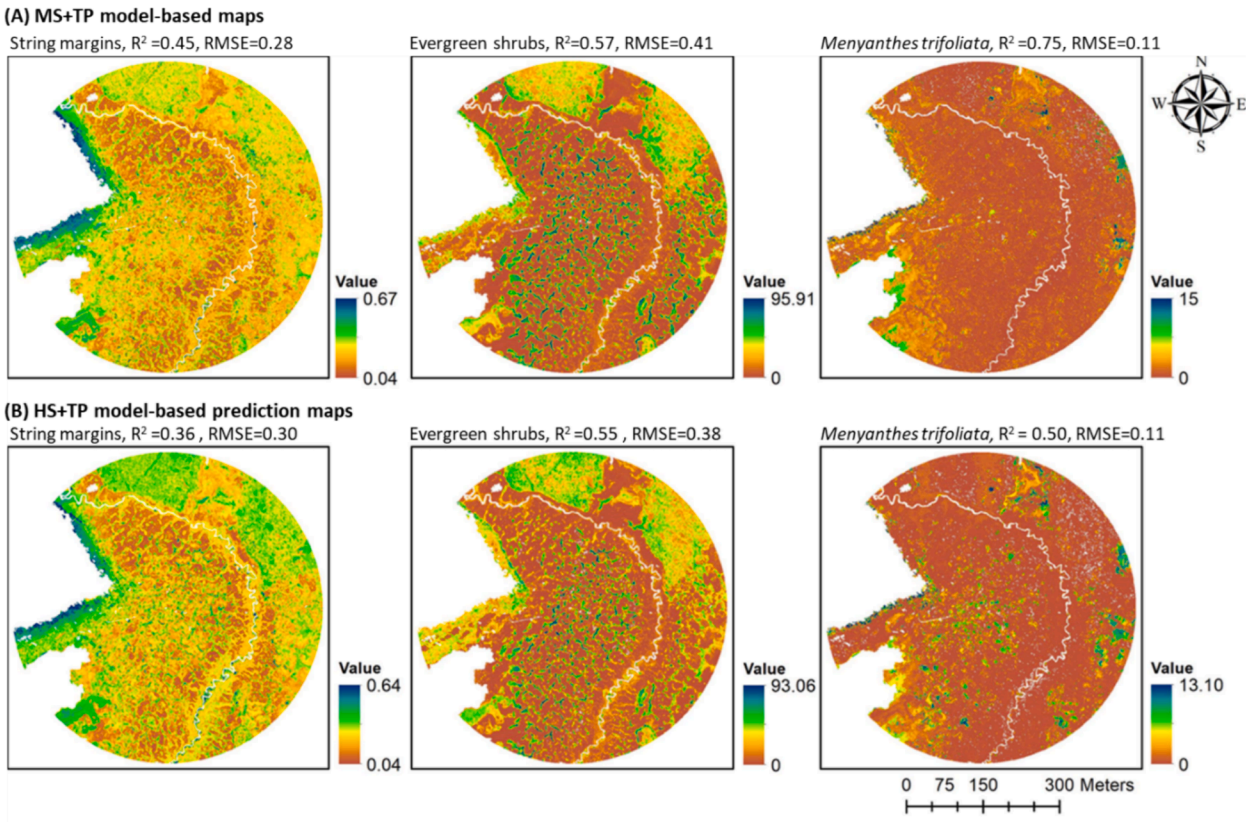

Fig. 7. Example vegetation maps based on (A row) MS+TP and (B row) HS+TP models in Kaamanen. Other predicted maps are shown in Appendix 3.

CRediT authorship contribution statement

Yuwen Pang: Writing – review & editing, Writing – original draft, Methodology, Funding acquisition, Formal analysis. **Aleksi Räsänen:** Writing – review & editing, Supervision, Conceptualization. **Franziska Wolff:** Writing – review & editing, Data curation. **Teemu Tahvanainen:** Writing – review & editing, Data curation. **Milja Männikkö:** Data curation. **Mika Aurela:** Writing – review & editing, Funding acquisition, Data curation. **Pasi Korpelainen:** Data curation. **Timo Kumpula:** Writing – review & editing, Funding acquisition. **Tarmo Virtanen:** Writing – review & editing, Supervision, Project administration, Funding acquisition, Conceptualization.

Declaration of competing interest

The authors declare that they have no known competing financial interests or personal relationships that could have appeared to influence the work reported in this paper.

Data availability

Data will be made available on request.

Acknowledgements

We thank Tiina H. M. Kolari, Viivi Lindholm, and Aino Syrjänen for assistance in fieldwork; the Chinese Scholarship Council (No. 202008330336) and the Academy of Finland (Grant nos. 308513, 349193, 330319, and 347860) for funding; and the CSC - IT Center for Science, Finland, for computational resources. Open access funded by Helsinki University Library.

Appendix A. Supplementary data

Supplementary data to this article can be found online at https://doi.org/10.1016/j.jag.2024.104043.

References

Aasen, H., Honkavaara, E., Lucieer, A., Zarco-Tejada, P.J., 2018. Quantitative remote sensing at ultra-high resolution with UAV spectroscopy: a review of sensor technology, measurement procedures, and data correction workflows. Remote Sensing 10.

Abdelmajeed, A.Y.A., Juszczak, R., 2024. Challenges and limitations of remote sensing applications in northern peatlands: present and future prospects. Remote Sensing 16, 591.

Adam, E., Mutanga, O., Rugege, D., 2010. Multispectral and hyperspectral remote sensing for identification and mapping of wetland vegetation: a review. Wetlands Ecology and Management 18, 281–296.

Andersen, R., Poulin, M., Borcard, D., Laiho, R., Laine, J., Vasander, H., Tuittila, E.T., 2011. Environmental control and spatial structures in peatland vegetation. Journal of Vegetation Science 22, 878–890.

Arasumani, M., Thiel, F., Pham, V.D., Hellmann, C., Kaiser, M., van der Linden, S., 2023. Advancing peatland vegetation mapping by spaceborne imaging spectroscopy. Ecological Indicators 154.

Assiri, M., Sartori, A., Persichetti, A., Miele, C., Faelga, R.A., Blount, T., Silvestri, S., 2023. Leaf area index and aboveground biomass estimation of an alpine peatland with a UAV multi-sensor approach. Giscience & Remote Sensing 60.

Assmann, J.J., Kerby, J.T., Cunliffe, A.M., Myers-Smith, I.H., 2019. Vegetation monitoring using multispectral sensors - best practices and lessons learned from high latitudes. Journal of Unmanned Vehicle Systems 7, 54–75.

BAATZ, M. & SCHÄPE, A. Multiresolution Segmentation: an optimization approach for high quality multi-scale image segmentation. 2000. 12-23.

Baird, A.J., Milner, A.M., Blundell, A., Swindles, G.T., Morris, P.J., 2016. Microform-scale variations in peatland permeability and their ecohydrological implications. Journal of Ecology 104, 531–544.

Behnamian, A., Millard, K., Banks, S.N., White, L., Richardson, M., Pasher, J., 2017. A systematic approach for variable selection with random forests: achieving stable variable importance values. Ieee Geoscience and Remote Sensing Letters 14, 1988–1992.

Belgiu, M., Dragut, L., 2016. Random forest in remote sensing: A review of applications and future directions. Isprs Journal of Photogrammetry and Remote Sensing 114, 24–31.

Berhane, T.M., Lane, C.R., Wu, Q.S., Anenkhonov, O.A., Chepinoga, V.V., Autrey, B.C., Liu, H.X., 2018. Comparing pixel- and object-based approaches in effectively classifying wetland-dominated landscapes. Remote Sensing 10.
Bertacchi, A., Giannini, V., di Franco, C., Silvestri, N., 2019. Using unmanned aerial vehicles for vegetation mapping and identification of botanical species in wetlands. Landscape and Ecological Engineering 15, 231–240.
Beyer, F., Jurasinski, G., Couwenberg, J., Grenzdorffer, G., 2019. Multisensor data to derive peatland vegetation communities using a fixed-wing unmanned aerial vehicle. International Journal of Remote Sensing 40, 9103–9125.
Blaschke, T., Hay, G.J., Kelly, M., Lang, S., Hofmann, P., Addink, E., Feitosa, R.Q., van der Meer, F., van der Werff, H., van Coillie, F., Tiede, D., 2014. Geographic object-based image analysis - towards a new paradigm. Isprs Journal of Photogrammetry and Remote Sensing 87, 180–191.
Borsoi, R., Imbiriba, T., Bermudez, J.C., Richard, C., Chanussot, J., Drumetz, L., Tourneret, J.Y., Zare, A., Jutten, C., 2021. Spectral variability in hyperspectral data unmixing. Ieee Geoscience and Remote Sensing Magazine 9, 223–270.
Breiman, L., 2001. Random forests. Machine Learning 45, 5–32.
Campello, R.J.G.B., Hruschka, E.R., 2006. A fuzzy extension of the silhouette width criterion for cluster analysis. Fuzzy Sets and Systems 157, 2858–2875.
Carter, G.A., 1994. Ratios of leaf reflectances in narrow wavebands as indicators of plant stress. International Journal of Remote Sensing 15, 697–703.
Conrad, O., Bechtel, B., Bock, M., Dietrich, H., Fischer, E., Gerlitz, L., Wehberg, J., Wichmann, V., Böhner, J., 2015. System for Automated Geoscientific Analyses (SAGA) v. 2.1.4. Geoscientific Model Development 8, 1991–2007.
Dahiya, N., Singh, S., Gupta, S., 2023. A review on deep learning classifier for hyperspectral imaging. International Journal of Image and Graphics 23.
de Caceres, M., Jansen, F., de Caceres, M.M., 2020. Package 'indicspecies'. Indicators 8, 1.
Diaz-Varela, R.A., Iglesias, S.C., Castro, C.C., Varela, E.R.D., 2018. Sub-metric analisis of vegetation structure in bog-heathland mosaics using very high resolution rpas imagery. Ecological Indicators 89, 861–873.
Dronova, I., Kislik, C., Dinh, Z., Kelly, M., 2021. A review of unoccupied aerial vehicle use in wetland applications: emerging opportunities in approach, technology, and data. Drones 5.
Du, B.J., Mao, D.H., Wang, Z.M., Qiu, Z.Q., Yan, H.Q., Feng, K.D., Zhang, Z.B., 2021. Mapping wetland plant communities using unmanned aerial vehicle hyperspectral imagery by comparing object/pixel-based classifications combining multiple machine-learning algorithms. Ieee Journal of Selected Topics in Applied Earth Observations and Remote Sensing 14, 8249–8258.
Durgan, S.D., Zhang, C.Y., Duecaster, A., Fourney, F., Su, H.B., 2020. Unmanned aircraft system photogrammetry for mapping diverse vegetation species in a heterogeneous coastal wetland. Wetlands 40, 2621–2633.
Erudel, T., Fabre, S., Houet, T., Mazier, F., Briottet, X., 2017. Criteria comparison for classifying peatland vegetation types using in situ hyperspectral measurements. Remote Sensing 9.
Ferraro, M.B., Giordani, P., Serafini, A., 2019. fclust: An R package for fuzzy clustering. R J. 11, 198.
Genuer, R., Poggi, J.M., Tuleau-Malot, C., 2015. VSURF: An R package for variable selection using random forests. R Journal 7, 19–33.
Gitelson, A.A., Zur, Y., Chivkunova, O.B., Merzlyak, M.N., 2002. Assessing carotenoid content in plant leaves with reflectance spectroscopy. Photochemistry and Photobiology 75, 272–281.
Hall, E.C., Lara, M.J., 2022. Multisensor UAS mapping of plant species and plant functional types in midwestern grasslands. Remote Sensing 14.
Harris, A., Baird, A.J., 2019. Microtopographic drivers of vegetation patterning in blanket peatlands recovering from erosion. Ecosystems 22, 1035–1054.
Harris, A., Charnock, R., Lucas, R.M., 2015. Hyperspectral remote sensing of peatland floristic gradients. Remote Sensing of Environment 162, 99–111.
Harris, L.I., Roulet, N.T., Moore, T.R., 2020. Mechanisms for the development of microform patterns in peatlands of the Hudson bay lowland. Ecosystems 23, 741–767.
Heiskanen, L., Tuovinen, J.P., Räsänen, A., Virtanen, T., Juutinen, S., Lohila, A., Penttilä, T., Linkosalmi, M., Mikola, J., Laurila, T., Aurela, M., 2021. Carbon dioxide and methane exchange of a patterned subarctic fen during two contrasting growing seasons. Biogeosciences 18, 873–896.
Hennessy, A., Clarke, K., Lewis, M., 2020. Hyperspectral classification of plants: a review of waveband selection generalisability. Remote Sensing 12.
Hijmans, R.J., 2018. raster: Geographic data analysis and modeling. R Package Version 2, 8.
Hossain, M.D., Chen, D., 2019. Segmentation for object-based image analysis (OBIA): A review of algorithms and challenges from remote sensing perspective. Isprs Journal of Photogrammetry and Remote Sensing 150, 115–134.
Hoyos-Santillan, J., Lomax, B.H., Large, D., Turner, B.L., Lopez, O.R., Boom, A., Sepulveda-Jauregui, A., Sjogersten, S., 2019. Evaluation of vegetation communities, water table, and peat composition as drivers of greenhouse gas emissions in lowland tropical peatlands. Science of the Total Environment 688, 1193–1204.
Isoaho, A., Ikkala, L., Pakkila, L., Marttila, H., Kareksela, S., Rasanen, A., 2024. Multi-sensor satellite imagery reveals spatiotemporal changes in peatland water table after restoration. Remote Sensing of Environment 306.
Jafarzadeh, H., Mahdianpari, M., Gill, E.W., Brisco, B., Mohammadimanesh, F., 2022. Remote Sensing and Machine Learning Tools to Support Wetland Monitoring: A Meta-Analysis of Three Decades of Research. Remote Sensing 14.
Kaneko, K., Yokochi, M., Inoue, T., Kato, Y., Fujita, H., 2024. Topographic conditions as governing factors of mire vegetation types analyzed from drone-based terrain model. Journal of Vegetation Science 35.
Kolari, T.H.M., Sallinen, A., Wolff, F., Kumpula, T., Tolonen, K., Tahvanainen, T., 2021. Ongoing fen-bog transition in a boreal aapa mire inferred from repeated field sampling, aerial images, and landsat data. Ecosystems.
Kopecky, M., Macek, M., Wild, J., 2021. Topographic Wetness Index calculation guidelines based on measured soil moisture and plant species composition. Science of the Total Environment 757.
Kotaridis, I., Lazaridou, M., 2021. Remote sensing image segmentation advances: A meta-analysis. Isprs Journal of Photogrammetry and Remote Sensing 173, 309–322.
Kou, D., Virtanen, T., Treat, C.C., Tuovinen, J.P., Räsänen, A., Juutinen, S., Mikola, J., Aurela, M., Heiskanen, L., Heikkilä, M., Weckström, J., Juselius, T., Piilo, S.R., Deng, J., Zhang, Y., Chaudhary, N., Huang, C.H., Väliranta, M., Biasi, C., Liu, X.Y., Guo, M.Y., Zhuang, Q.L., Korhola, A., Shurpali, N.J., 2022. Peatland Heterogeneity Impacts on Regional Carbon Flux and Its Radiative Effect Within a Boreal Landscape. Journal of Geophysical Research-Biogeosciences 127.
Kupkova, L., Cervena, L., Potuckova, M., Lysak, J., Roubalova, M., Hrazsky, Z., Brezina, S., Epstein, H.E., Mullerova, J., 2023. Towards reliable monitoring of grass species in nature conservation: Evaluation of the potential of UAV and PlanetScope multi-temporal data in the Central European tundra. Remote Sensing of Environment 294.
Lehnert, L.W., Meyer, H., Obermeier, W.A., Silva, B., Regeling, B., Thies, B., Bendix, J., 2019. Hyperspectral data analysis in R: The hsdar Package. Journal of Statistical Software 89.
Li, H.D., Cui, J., Zhang, X.L., Han, Y.Q., Cao, L.Y., 2022. Dimensionality reduction and classification of hyperspectral remote sensing image feature extraction. Remote Sensing 14.
LI, Q. S., WONG, F. K. K. & FUNG, T. 2017. Assessing the Utility of Uav-Borne Hyperspectral Image and Photogrammetry Derived 3d Data for Wetland Species Distribution Quick Mapping. *International Conference on Unmanned Aerial Vehicles in Geomatics (Volume Xlii-2/W6),* 42-2, 209-215.
Li, Y.F., Yu, Z.C., Wang, M., Li, H.K., Sun, J.J., Wang, S.Z., 2024. Control of local topography and surface patterning on the formation and stability of a slope permafrost peatland at 4800-m elevation on the central Qinghai-Tibetan Plateau. Ecological Indicators 158.
Liaw, A., Wiener, M., 2002. Classification and regression by randomForest. R News 2, 18–22.
Linkosalmi, M., Tuovinen, J.P., Nevalainen, O., Peltoniemi, M., Tanis, C.M., Arslan, A.N., Rainne, J., Lohila, A., Laurila, T., Aurela, M., 2022. Tracking vegetation phenology of pristine northern boreal peatlands by combining digital photography with CO2 flux and remote sensing data. Biogeosciences 19, 4747–4765.
Loisel, J., van Bellen, S., Pelletier, L., Talbot, J., Hugelius, G., Karran, D., Yu, Z.C., Nichols, J., Holmquist, J., 2017. Insights and issues with estimating northern peatland carbon stocks and fluxes since the Last Glacial Maximum. Earth-Science Reviews 165, 59–80.
Lovitt, J., Rahman, M.M., Saraswati, S., McDermid, G.J., Strack, M., Xu, B., 2018. UAV remote sensing can reveal the effects of low-impact seismic lines on surface morphology, hydrology, and methane (CH4) release in a boreal treed bog. Journal of Geophysical Research-Biogeosciences 123, 1117–1129.
Ma, L., Cheng, L., Li, M.C., Liu, Y.X., Ma, X.X., 2015. Training set size, scale, and features in geographic object-based image analysis of very high resolution unmanned aerial vehicle imagery. Isprs Journal of Photogrammetry and Remote Sensing 102, 14–27.
Maanavilja, L., Riutta, T., Aurela, M., Pulkkinen, M., Laurila, T., Tuittila, E.S., 2011. Spatial variation in CO2 exchange at a northern aapa mire. Biogeochemistry 104, 325–345.
Marcello, J., Eugenio, F., Perdomo, U., Medina, A., 2016. Assessment of atmospheric algorithms to retrieve vegetation in natural protected areas using multispectral high resolution Imagery. Sensors 16.
Marcinkowska-Ochtyra, A., Jarocinska, A., Bzdega, K., Tokarska-Guzik, B., 2018. Classification of expansive grassland species in different growth stages based on hyperspectral and LiDAR data. Remote Sensing 10.
Maxwell, A.E., Warner, T.A., Fang, F., 2018. Implementation of machine-learning classification in remote sensing: an applied review. International Journal of Remote Sensing 39, 2784–2817.
McPartland, M.Y., Falkowski, M.J., Reinhardt, J.R., Kane, E.S., Kolka, R., Turetsky, M.R., Douglas, T.A., Anderson, J., Edwards, J.D., Palik, B., Montgomery, R.A., 2019. Characterizing boreal peatland plant composition and species diversity with hyperspectral remote sensing. Remote Sensing 11.
Middleton, M., Narhi, P., Arkimaa, H., Hyvonen, E., Kuosmanen, V., Treitz, P., Sutinen, R., 2012. Ordination and hyperspectral remote sensing approach to classify peatland biotopes along soil moisture and fertility gradients. Remote Sensing of Environment 124, 596–609.
Mörsky, S.K., Haapala, J.K., Rinnan, R., Saarnio, S., Suokanerva, H., Latola, K., Kyro, E., Silvola, J., Holopainen, T., Martikainen, P.J., 2012. Minor long-term effects of ultraviolet-B radiation on methane dynamics of a subarctic fen in Northern Finland. Biogeochemistry 108, 233–243.
Oksanen, J., Blanchet, F.G., Kindt, R., Legendre, P., Minchin, P.R., O'Hara, R., Simpson, G.L., Solymos, P., Stevens, M.H.H., Wagner, H., 2020. Package 'vegan'. Community Ecology Package, Version 2, 1–295.
Oldeland, J., Revermann, R., Luther-Mosebach, J., Buttschardt, T., Lehmann, J.R.K., 2021. New tools for old problems - comparing drone- and field-based assessments of a problematic plant species. Environmental Monitoring and Assessment 193.
Pang, Y.W., Räsänen, A., Lindholm, V., Aurela, M., Virtanen, T., 2022. Detecting peatland vegetation patterns with multi-temporal field spectroscopy. Giscience & Remote Sensing 59, 2111–2126.
Peddle, D.R., White, H.P., Soffer, R.J., Miller, J.R., Ledrew, E.F., 2001. Reflectance processing of remote sensing spectroradiometer data. Computers & Geosciences 27, 203–213.

Pedregosa, F., Varoquaux, G., Gramfort, A., Michel, V., Thirion, B., Grisel, O., Blondel, M., Prettenhofer, P., Weiss, R., Dubourg, V., Vanderplas, J., Passos, A., Cournapeau, D., Brucher, M., Perrot, M., Duchesnay, E., 2011. Scikit-learn: machine learning in python. Journal of Machine Learning Research 12, 2825–2830.

Plaza, A., Benediktsson, J.A., Boardman, J.W., Brazile, J., Bruzzone, L., Camps-Valls, G., Chanussot, J., Fauvel, M., Gamba, P., Gualtieri, A., Marconcini, M., Tilton, J.C., Trianni, G., 2009. Recent advances in techniques for hyperspectral image processing. Remote Sensing of Environment 113, S110–S122.

Prentice, R.M., Villoslada Pecina, M., Ward, R.D., Bergamo, T.F., Joyce, C.B., Sepp, K., 2021. machine learning classification and accuracy assessment from high-resolution images of coastal wetlands. Remote Sensing 13.

Putkiranta, P., Räsänen, A., Korpelainen, P., Erlandsson, R., Kolari, T.H., Pang, Y., Villoslada, M., Wolff, F., Kumpula, T., Virtanen, T., 2024. The value of hyperspectral UAV imagery in characterizing tundra vegetation. Remote Sensing of Environment 308, 114175.

Räsänen, A., Rusanen, A., Kuitunen, M., Lensu, A., 2013. What makes segmentation good? A case study in boreal forest habitat mapping. International Journal of Remote Sensing 34, 8603–8627.

Räsänen, A., Juutinen, S., Tuittila, E.S., Aurela, M., Virtanen, T., 2019. Comparing ultra-high spatial resolution remote-sensing methods in mapping peatland vegetation. Journal of Vegetation Science 30, 1016–1026.

Räsänen, A., Virtanen, T., 2019. Data and resolution requirements in mapping vegetation in spatially heterogeneous landscapes. Remote Sensing of Environment 230.

Räsänen, A., Aurela, M., Juutinen, S., Kumpula, T., Lohila, A., Penttila, T., Virtanen, T., 2020a. Detecting northern peatland vegetation patterns at ultra-high spatial resolution. Remote Sensing in Ecology and Conservation 6, 457–471.

Räsänen, A., Juutinen, S., Kalacska, M., Aurela, M., Heikkinen, P., Maenpaa, K., Rimali, A., Virtanen, T., 2020b. Peatland leaf-area index and biomass estimation with ultra-high resolution remote sensing. Giscience & Remote Sensing 57, 943–964.

Räsänen, A., Tolvanen, A., Kareksela, S., 2022. Monitoring peatland water table depth with optical and radar satellite imagery. International Journal of Applied Earth Observation and Geoinformation 112.

Rupp, D., Kane, E.S., Dieleman, C., Keller, J.K., Turetsky, M., 2019. Plant functional group effects on peat carbon cycling in a boreal rich fen. Biogeochemistry 144, 305–327.

Rydin, H., Jeglum, J.K., 2013. The Biology of Peatlands. Oxford University Press.

Rydin, H., Jeglum, J.K., Rydin, H., Jeglum, J.K., 2006. Peatland patterns and landforms. Oxford University Press, The Biology of Peatlands.

Salamí, E., Barrado, C., Pastor, E., 2014. UAV flight experiments applied to the remote sensing of vegetated areas. Remote Sensing 6, 11051–11081.

Simpson, G., Nichol, C.J., Wade, T., Helfter, C., Hamilton, A., Gibson-Poole, S., 2024. Species-level classification of peatland vegetation using ultra-high-resolution UAV imagery. Drones 8, 97.

Steenvoorden, J., Bartholomeus, H., Limpens, J., 2023. Less is more: Optimizing vegetation mapping in peatlands using unmanned aerial vehicles (UAVs). International Journal of Applied Earth Observation and Geoinformation 117.

Swanson, D.K., Grigal, D.F., 1988. A simulation-model of mire patterning. *Oikos* 53, 309–314.

Szporak-Wasilewska, S., Piórkowski, H., Ciezkowski, W., Jarzombkowski, F., Slawik, L., Kopec, D., 2021. Mapping alkaline fens, transition mires and quaking bogs using airborne hyperspectral and laser scanning data. Remote Sensing 13.

Villoslada, M., Berner, L.T., Juutinen, S., Ylänne, H., Kumpula, T., 2024. Upscaling vascular aboveground biomass and topsoil moisture of subarctic fens from Unoccupied Aerial Vehicles (UAVs) to satellite level. Science of the Total Environment 933, 173049.

Wang, C., Pavelsky, T. M., Kyzivat, E. D., Garcia-Tigreros, F., Podest, E., Yao, F. F., Yang, X., Zhang, S., Song, C. H., Langhorst, T., Dolan, W., Kurek, M. R., Harlan, M. E., Smith, L. C., Butman, D. E., Spencer, R. G. M., Gleason, C. J., Wickland, K. P., Striegl, R. G. & Peters, D. L. 2023. Quantification of wetland vegetation communities features with airborne AVIRIS-NG, UAVSAR, and UAV LiDAR data in Peace-Athabasca Delta. *Remote Sensing of Environment,* 294.

Wang, C.Y., Myint, S.W., 2015. A simplified empirical line method of radiometric calibration for small unmanned aircraft systems-based remote sensing. Ieee Journal of Selected Topics in Applied Earth Observations and Remote Sensing 8, 1876–1885.

Wengert, M., Wijesingha, J., Schulze-Brüninghoff, D., Wachendorf, M., Astor, T., 2022. Multisite and multitemporal grassland yield estimation using UAV-borne hyperspectral data. Remote Sensing 14.

Witharana, C., Civco, D.L., 2014. Optimizing multi-resolution segmentation scale using empirical methods: Exploring the sensitivity of the supervised discrepancy measure Euclidean distance 2 (ED2). Isprs Journal of Photogrammetry and Remote Sensing 87, 108–121.

Wolff, F., Kolari, T. H. M., Villoslada, M., Tahvanainen, T., Korpelainen, P., Zamboni, P. A. P. & Kumpula, T. 2023. RGB vs. Multispectral imagery: Mapping aapa mire plant communities with UAVs. *Ecological Indicators,* 148.

Wu, S.J., Tetzlaff, D., Daempfling, H., Soulsby, C., 2023. Improved understanding of vegetation dynamics and wetland ecohydrology via monthly UAV-based classification. Hydrological Processes 37.

Yu, Z.C., 2012. Northern peatland carbon stocks and dynamics: a review. Biogeosciences 9, 4071–4085.

Zhang, Y.S., Odeh, I.O.A., Liu, B., Wang, X.Q., 2018. Subpixel mapping and confusion matrix analysis of plant functional types in peatlands using MESMA applied to AISA Eagle imagery. Journal of Applied Remote Sensing 12.

Zhang, L.F., Zhang, L.P., 2022. Artificial intelligence for remote sensing data analysis. A review of challenges and opportunities. Ieee Geoscience and Remote Sensing Magazine 10, 270–294.

Zhou, R., Yang, C., Li, E.H., Cai, X.B., Yang, J., Xia, Y., 2021. Object-based wetland vegetation classification using multi-feature selection of unoccupied aerial vehicle RGB imagery. Remote Sensing 13.